# The Nonmutagenic (*R*)- and (*S*)-β-(*N*$^6$-Adenyl)styrene Oxide Adducts Are Oriented in the Major Groove and Show Little Perturbation to DNA Structure†

Christophe Hennard,‡ Jari Finneman,§ Constance M. Harris, Thomas M. Harris, and Michael P. Stone*

*Department of Chemistry and Center in Molecular Toxicology, Vanderbilt University, Nashville, Tennessee 37235*

*Received March 20, 2001; Revised Manuscript Received June 11, 2001*

ABSTRACT: Conformations of (*R*)-β-(*N*$^6$-adenyl)styrene oxide and (*S*)-β-(*N*$^6$-adenyl)styrene oxide adducts at position X$^6$ in d(CGGACXAGAAG)·d(CTTCTTGTCCG), incorporating codons 60, 61 (underlined), and 62 of the human *N-ras* protooncogene, were refined from $^1$H NMR data. These were designated as the β-R(61,2) and β-S(61,2) adducts. A total of 533 distance restraints and 162 dihedral restraints were used for the molecular dynamics calculations of the β-S(61,2) adduct, while 518 distances and 163 dihedrals were used for the β-R(61,2) adduct. The increased tether length of the β-adducts results in two significant changes in adduct structure as compared to the corresponding α-styrenyl adducts [Stone, M. P., and Feng, B. (1996) *Magn. Reson. Chem. 34*, S105−S114]. First, it reduces the distortion introduced into the DNA duplex. For both the β-R(61,2) and β-S(61,2) adducts, the styrenyl moiety was positioned in the major groove of the duplex with little steric hindrance. Second, it mutes the influence of stereochemistry at the α-carbon such that both the β-R(61,2) and β-S(61,2) adducts exhibit similar conformations. The results were correlated with site-specific mutagenesis experiments that revealed the β-R(61,2) and β-S(61,2) adducts were not mutagenic and did not block polymerase bypass.

Styrene is a mutagen in prokaryotes (*1*−*3*) and eukaryotes (*4*). It is of concern as a potential human mutagen (*5*−*9*). Styrene genotoxicity results from cytochrome P$_{450}$-mediated metabolism to the ultimate carcinogenic species, styrene oxide (SO)[1] (*10*−*17*). SO induces sister chromosome exchange and aberrations in human lymphocytes in vitro (*18*, *19*). Adducts of SO at guanine O$^6$ and guanine N$^2$ were identified in human cells (*20*−*23*). Increased levels of the guanine O$^6$ adduct, a potential biomarker for styrene exposure, were observed in lamination workers chronically exposed to styrene in the plastics industry (*24*). Molecular analysis of mutations at the hypoxanthine-guanine phosphoribosyl transferase (*hprt*) gene in peripheral blood lymphocytes suggested that they occurred at both guanine and adenine sites, and were predominantly base pair substitutions (*25*). The occurrence of guanine O$^6$ adducts did not strongly correlate with the frequency of *hprt* mutations (*24*). This suggested that the guanine O$^6$ SO adducts were weakly mutagenic. Alternatively, they were perhaps not the source of the mutations. Thus, the relationship between styrene-induced DNA damage and mutagenesis remains to be established (*23*).

The reactivity of styrene oxide with DNA is complex. This electrophile reacts in vitro to form adducts at a number of nucleophilic sites for both deoxyguanosine and deoxyadenosine (*26*, *27*). In principle, reaction may proceed via either the α- or β-carbons of the epoxide. The β-adducts at adenine N$^6$ arise solely by a mechanism involving attack on the oxirane by the N1 position of deoxyadenosine, followed by Dimroth rearrangement (*28*, *29*). This contrasts with the α-adducts at adenine N$^6$ which primarily undergo direct reaction between the exocyclic amino group and the α-carbon atom of the oxirane (*27*, *29*). Alternatively, the imino nitrogen of deoxyadenosine can react with the α-carbon, to yield the α-N1 adduct, followed by Dimroth rearrangement to the corresponding α-N$^6$ adduct (*28*).

Cells containing activated oncogenes often contain mutations in *ras* (*30*). Mutations within codon 61 cause oncogene activation (*31*). The *ras61* oligodeoxynucleotide 5′-d(CGGACAAGAAG)-3′·5′-d(CTTCTTGTCCG)-3′ (*32*) provides a model with which to simultaneously examine site-specific mutagenesis of styrene oxide adenine N$^6$ lesions (*33*), replication bypass of adenine N$^6$ lesions in vitro (*34*, *35*), and the solution structures of adenine N$^6$ lesions (*36*−*40*). These studies are facilitated by large-scale production of site-specifically modified oligodeoxynucleotides (*41*).

Previous studies were performed on the α-adenine N$^6$ adducts of styrene oxide. The α-R(61,2) adduct provided a replication block to a variety of polymerases. The α-S(61,2) lesion was weakly mutagenic, yielding low levels of A → G transitions (*33*). This was the most frequently observed SO-induced *hprt* mutation in human lymphocytes (*25*), which

† This work was supported by NIH Grants ES-05509 (T.M.H.) and ES-05355 (M.P.S.). Funding for the NMR spectrometer was supplied by NIH Grant RR-05805 and the Vanderbilt Center in Molecular Toxicology (Grant ES-00267). The National Magnetic Resonance Facility at Madison was funded by the University of Wisconsin, NSF Grants DMB-8415048 and BIR-9214394, NIH Grants RR-02301, RR-02781, and RR08438, and the USDA.

* To whom correspondence should be addressed. Phone: (615) 322-2589. Fax: (615) 343-1234. E-mail: stone@toxicology.mc.vanderbilt.edu.

‡ Current address: European Patent Office, Munich, Germany.

§ Current address: Pfizer, Inc., Groton, CT 06340.

[1] Abbreviations: DSS, sodium 4,4-dimethyl-4-silapentanesulfonate; EDTA, ethylenediaminetetraacetic acid; HPLC, high-pressure liquid chromatography; MALDI-TOF, matrix-assisted laser desorption ionization time-of-flight mass spectrometry; NMR, nuclear magnetic resonance; NOE, nuclear Overhauser enhancement; NOESY, two-dimensional NOE spectroscopy; SO, styrene oxide; TPPI, time-proportional phase increment; TOCSY, total homonuclear correlated spectroscopy; 1D, one-dimensional; 2D, two-dimensional.

10.1021/bi010564v CCC: $20.00 
Published on Web 07/25/2001

Chart 1: Structures of the (*R*)- and (*S*)-β-(*N*$^6$-Adenyl)styrene Oxide Adducts

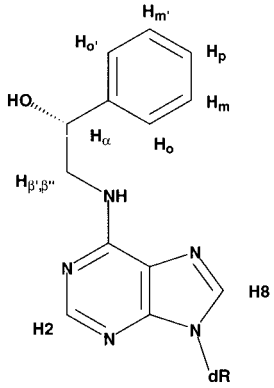


**R-β-(N$^6$-adenyl)-styrene oxide adduct**

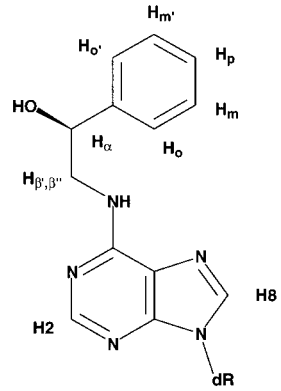


**S-β-(N$^6$-adenyl)-styrene oxide adduct**

suggested the potential importance of the adenyl N$^6$ lesions in understanding the toxicology of SO. Thus, while the guanine O$^6$ adducts potentially provide a biomarker of exposure, the less common adenine N$^6$ lesions might be more mutagenic (*25*). The bulkier and intercalating adenyl N$^6$ adducts of benzo[*a*]pyrene (*42*) and benz[*a*]anthracene (*43*) also yielded A → G mutations in this site-specific mutagenesis assay, but at higher levels.

Structural studies of the α-adenine N$^6$ adducts in the *ras61* oligodeoxynucleotide were correlated with site-specific mutagenesis studies. The unmodified oligodeoxynucleotide (*32*) existed as a right-handed B-DNA-like duplex. The structures of the α-R(61,2) and α-S(61,2) α-styrene oxide lesions (*36*−*38*) revealed the influence of stereochemistry in determining adduct orientation. The *R*-diastereomer was oriented in the 5′-direction, while the *S*-diastereomer was oriented in the 3′-direction from the lesion site. Subsequent studies examined the α-R(61,2) and α-S(61,2) adducts placed opposite a mismatched cytosine (*40*). These were the α-R- and α-S(61,2)C adducts. These studies suggested that DNA sequence and base pair geometry may play a role in causing A → G mutations at the adduct site. The α-S(61,2)C adduct afforded a stable solution structure, while the α-R(61,2)C adduct resulted in a disordered structure. The phenyl ring of the styrene in the S(61,2)C adduct was in the major groove and remained oriented in the 3′-direction. A shift of the modified adenine toward the minor groove resulted in the styrenyl ring stacking with nucleotide C$^5$ on the 5′-side of the lesion, which shifted toward the major groove. Neither the S(61,2)C nor the R(61,2)C adduct formed protonated

Chart 2: β-R(61,2) and β-S(61,2) Oligodeoxynucleotides, Where R Is the (*R*)-β-(*N*$^6$-Adenyl)styrene Oxide Adduct and S Is the (*S*)-β-(*N*$^6$-Adenyl)styrene Oxide Adduct

ras codons

```
          60          61          62
5'-C1 |G2 G3 A4 |C5 R6 A7 |G8 A9 A10|G11-3'
3'-G22|C21C20T19|G18T17T16|C15T14T13|C12-5'

          60          61          62
5'-C1 |G2 G3 A4 |C5 S6 A7 |G8 A9 A10|G11-3'
3'-G22|C21C20T19|G18T17T16|C15T14T13|C12-5'
```

wobble A·C hydrogen bonds. This suggested that protonated wobble A·C pairing need not be a prerequisite for low levels of α-SO-induced A → G mutations. The shift of the modified adenine toward the minor groove in the S(61,2)C structure was proposed to contribute to the genesis of A → G mutations. The disordered structure of the α-R(61,2)C adduct provides a potential explanation for why that adduct does not induce A → G mutations.

In the work presented here, the synthetic method was extended to production of the (*R*)-β-(*N*$^6$-adenyl)styrene oxide and (*S*)-β-(*N*$^6$-adenyl)styrene oxide adducts (Chart 1) at position X$^6$ in 5′-d(CGGACXAGAAG)-3′·5′-d(CTTCTTGTCCG)-3′, where X is the adducted adenine. These were named the β-R(61,2) and β-S(61,2) adducts (Chart 2). The availability of β-adducts allowed the role of linker length between the exocyclic amino group of adenine and the phenyl ring of styrene oxide to be examined. The increased tether length results in two significant changes in structure of the β-styrenyl adducts as compared to the corresponding α-styrenyl adducts. First, it substantially reduces the distortion introduced into the DNA duplex. In both the β-R(61,2) and β-S(61,2) adducts, the styrenyl moiety was positioned in the major groove of the duplex with little steric hindrance. Second, it mutes the influence of stereochemistry at the α-carbon such that both the β-R(61,2) and β-S(61,2) adducts exhibit similar conformations. The results are correlated with site-specific mutagenesis experiments that revealed the β-R(61,2) and β-S(61,2) adducts were nonmutagenic. Moreover, replication studies in vitro showed that these two adducts did not pose significant replication blocks to a variety of polymerases (*44*).

## MATERIALS AND METHODS

*Sample Preparation*. The oligodeoxynucleotide d(CTTCTTGTCCG) was purchased from Midland Certified Reagent Co. (Midland, TX). The concentration of the single-stranded unmodified oligodeoxynucleotide was determined from the extinction coefficient of $9.08 \times 10^4$ M$^{-1}$ cm$^{-1}$ at 260 nm (*45*). The β-styrenyl-adducted oligodeoxynucleotide was prepared by reaction of 3.3 mg of (2*R*)- or (2*S*)-2-amino-1-phenylethanol (*40*) with 245 $A_{260}$ units of chloropurine-containing 11-mer (*41*), in 500 μL of anhydrous dimethyl sulfoxide containing 5 μL of diisopropylethylamine, for 24−70 h at 50 °C. The solvent was removed in vacuo. The residue was dissolved in 2 mL of $H_2O$. It was purified by HPLC using a YMC-ODS-AQ column (10 mm × 250 mm), at a flow rate of 5.0 mL/min, with a gradient of (a) 0.1 M ammonium formate (pH 6.3) and (b) acetonitrile, from 1 to

13% B over the course of 22 min. The retention time of the adducted oligodeoxynucleotide was 20.5 min. The duplex constructs were obtained by mixing the two complementary strains in a 10 mM phosphate buffer (pH 6.9). They were heated to 85 °C and cooled to room temperature before storage overnight at 4 °C. The duplex was purified from unannealed single strands by chromatography over a DNA grade Bio-Gel hydroxylapatite (Bio-Rad Laboratories, Richmond, CA) column and eluted with a gradient from 10 to 200 mM sodium phosphate buffer (pH 6.9). Trace amounts of metal were eliminated by washing the sample over Chelex 100 resin (Bio-Rad Laboratories). The resulting solution was evaporated under reduced pressure. A gel filtration column (G-25 Sephadex, Amersham-Pharmacia, Inc., Piscataway, NJ) was used to desalt the duplex before exchange with $D_2O$ for the NMR experiments. Samples were dissolved in 10 mM sodium phosphate buffer (pH 6.9) containing 100 mM NaCl and 0.05 mM $Na_2EDTA$ for the NMR measurements.

*Capillary Electrophoresis*. These were performed on a PACE 5500 (Beckman Instruments, Inc., Fullerton, CA) instrument using an eCAP ssDNA 100-R kit applying 12 000 V for 30 min. The electropherogram was monitored using a UV detector set at 254 nm. The electropherograms of the adducted duplex oligodeoxynucleotides exhibited two peaks in an approximate 1:1 ratio after correction for the respective absorbance coefficients at the measuring wavelength. In each instance, the retention times were 24.4 and 24.6 min.

*Mass Spectrometry*. MALDI-TOF spectra were measured on a Voyager-DE (PerSeptive Biosystems, Inc.) instrument in negative reflector mode. The sample was mixed with matrix in a 1:1 $CH_3CN/H_2O$ mixture, placed on a target plate, and allowed to dry. The matrix contained 0.5 M 3-hydroxypicolinic acid and 0.1 M ammonium tartrate. For each oligodeoxynucleotide duplex, mass measurement showed two signals, at 3520.3 and 3274.0 mass units. These corresponded to the styrene-adducted d(CGGACAAGAAG) strand (calculated mass of 3519.44 for $C_{116}H_{141}N_{51}O_{60}P_{10}$) and the d(CTTCTTGTCCG) strand (calculated mass of 3274.17 for $C_{106}H_{138}N_{32}O_{69}P_{10}$), respectively.

*UV Spectroscopy*. The NaCl concentration was adjusted to 1 M for the melt determinations. The melting temperature was determined by measuring the absorbance change at 260 nm as a function of temperature. The instrument that was used was a Varian Cary 4E UV−vis spectrophotometer (Varian Instruments, Walnut Creek, CA) equipped with a 12-position cell changer and a temperature controller. Three melting and three annealing curves were averaged. For these experiments, the temperature ranged from 15 to 75 °C with a 0.5 °C/min increment. A 3 nm bandwidth and a 5 s averaging time were used to reduce the level of fluctuations.

*Nuclear Magnetic Resonance.* Spectra were recorded at 500.13 MHz on a Bruker Avance DRX-500 spectrometer (Bruker Instruments, Billerica, MA). The sample used for the observation of the nonexchangeable protons was exchanged three times in 99.96% $D_2O$ and suspended in 0.5 mL of NMR buffer containing 99.996% $D_2O$, while that used for the observation of the exchangeable protons was dissolved in 0.5 mL of NMR buffer containing a 9:1 $H_2O/D_2O$ mixture. Spectra were referenced to the water resonance at 4.92 ppm at 10 °C or 4.81 ppm at 20 °C. Phase-sensitive NOESY spectra used for resonance assignments were recorded using TPPI quadrature detection. A mixing time of 200 ms was used with 1024 real points collected in the $t_1$ dimension, 32 scans per FID with a 2.0 s relaxation delay, and 2048 data points collected in the $t_2$ dimension. The water resonance was saturated during the relaxation delay and the mixing period. Data were zero-filled in the $t_1$ dimension to give a matrix of 2048 × 2048 data points. A sine-bell square apodization function with a 90° phase shift and a skew factor of 0.7 were used in the $t_1$ and $t_2$ dimensions. Phase-sensitive NOESY experiments carried out in a 9:1 $H_2O/D_2O$ mixture were performed using the WATERGATE water suppression pulse program (*46*). NMR data were transferred to Octane workstations (Silicon Graphics, Inc., Mountain View, CA) and processed using FELIX 97 software (Molecular Simulations, Inc., San Diego, CA).

*Restraints.* NOESY spectra at mixing times of 100, 150, and 200 ms were acquired within a single time period. Using FELIX, footprints were drawn around the cross-peaks for the spectrum measured with a mixing time of 200 ms. Those footprints were then transferred to the other spectra. Cross-peaks intensities were determined by volume integration of the areas under the footprints. In the case of extreme overlap, the volumes were estimated. B-DNA and A-DNA models were constructed and used as reference structures. The models were made from B- or A-DNA (*47*) to which the styrene $\beta$-carbon was bonded to the $N^6$ of $A^6$ with the correct stereochemistry. The aromatic ring of the styrene was placed in the major groove of the DNA in all cases. The models were then energy-minimized to give the starting structures for the subsequent calculations.

*Distance Restraints.* MARDIGRAS (*48*, *49*) was used to iteratively refine the matrix and optimize the agreement between the calculated and experimental NOE intensities. The NOE intensities were combined with those generated from the complete relaxation matrix analysis of a starting DNA structure to generate a hybrid intensity matrix. Isotropic correlation times of 2, 3, and 4 ns for both the sugar and base protons were used in combination with the two DNA starting structures and the NOE experiments at three mixing times to yield 18 sets of distances. Average distances and standard deviations were calculated from these 18 sets of data and used as bounds for the NOE restraints used in the subsequent rMD calculations.

*Torsion Angle Restraints.* DQF-COSY spectra were recorded using 512 FIDs with 32 scans per spectra. The coupling constants of the sugar protons (H1′, H2′, and H2″) measured from this spectra using FELIX allowed us to determine the pseudorotation angle for each sugar and in turn calculate the torsion angles of the sugar rings. A $^1H-^{31}P$ COSY experiment was used to observe the chemical shifts of the phosphorus nuclei of the DNA backbone. The constants for coupling between H3′ and P were not determined, but the observation of the coupling was used to give empirical values to the $\epsilon$ and $\delta$ angles of the backbone (*50*).

*Restrained Molecular Dynamics.* Calculations were performed using X-PLOR (*51*). The force field was derived from CHARMM (*52*) and adapted for restrained MD calculations of nucleic acids. The empirical energy function was developed for nucleic acids and treated all hydrogens explicitly. It consisted of energy terms for bonds, bond angles, torsion angles, tetrahedral and planar geometry, hydrogen bonding, and nonbonded interactions, including van der Waals and electrostatic forces. All calculations were performed in vacuo

Table 1: Melting Temperatures of Styrene Adducts in the *ras61* Oligomer

| adduct | $T_m$ (±1 °C) | $\Delta T_m$ (°C) |
|---|---|---|
| *ras61* (unmodified) | 53 | |
| β-R(61,2) | 46 | 7 |
| β-S(61,2) | 48 | 5 |
| α-R(61,2) | 42 | 11 |
| α-S(61,2) | 36 | 17 |
| α-R(61,3) | 42 | 11 |
| α-S(61,3) | 42 | 11 |

without explicit counterions. The integration time step was 1 fs. The effective function included terms describing distance and dihedral restraints, which were in the form of square well potentials (*53*). The distance restraints were divided into five classes on the basis of the confidence factors. Watson−Crick hydrogen bonding restraints between base pairs were used.

Sets of rMD calculations were performed using both starting structures B and A. Random velocities fitting a Maxwell−Boltzmann distribution were assigned. During the calculations, the system was coupled to a heating bath with a target temperature of 2500 K maintained for 30 ps. The molecule was then cooled to 300 K in 5 ps and kept at that temperature for 15 ps. The force constants were initially set to 50, 45, 40, 35, and 30 in the order of the confidence factor and kept for 10 ps, before they were scaled up to 200, 180, 160, 140, and 120, respectively, over a 10 ps period. These levels were maintained for 17 ps, then scaled to 150, 140, 130, 120, and 110, respectively, over a 3 ps period, and maintained for an additional 10 ps for the final equilibration step. Back calculation of the theoretical NMR intensities from the final structures was performed using CORMA (*54*).

## RESULTS

*Sample Properties*. The duplex melting temperatures were compared to that of the unmodified *ras61* duplex, and to those of the corresponding α-R(61,2) and α-S(61,2) styrene oxide-modified duplexes. The significant observation was that the β-R(61,2) and β-S(61,2) adducts caused substantially less thermal destabilization than the corresponding α-adducts of styrene oxide. A decrease of 5 °C for the β-S(61,2) adduct was observed, while the β-R(61,2) adduct had a 7 °C lower melting temperature; thus, the melting temperatures are 48 and 46 °C, respectively (Table 1). This may be compared with the 11 °C decrease in $T_m$ for the α-R(61,2) adduct and the 17 °C decrease in $T_m$ for the α-S(61,2) adduct. Sample NMR spectra were acquired under various conditions. It was determined that the temperature range of 10−20 °C provided the optimal temperature for NMR spectroscopy experiments.

*DNA Resonance Assignments*. The spectral assignments of the nonexchangeable protons were made using the NOESY (*55*, *56*) and COSY spectra at 10 °C in the case of the β-S(61,2) adduct and at 20 °C in the case of the β-R(61,2) adduct. The assignment of the H1′ and base protons led to the subsequent assignment of the other sugar protons. An expanded NOESY spectrum shows connectivities between the base and anomeric H1′ protons (Figure 1). Two notable features were observed for each adduct. First, the sequential NOEs were complete and did not exhibit unusual intensities, suggesting minimal perturbation of the DNA duplex by these adducts. Second, both the β-R(61,2) and β-S(61,2) styrenyl adducts caused significant upfield shifts for the aromatic H5 and H6 protons of $C^5$. This is the 5′-neighbor to the adducted base $X^6$. These upfield shifts were attributed to ring current shielding by the phenyl ring of the styrenyl adduct. The result

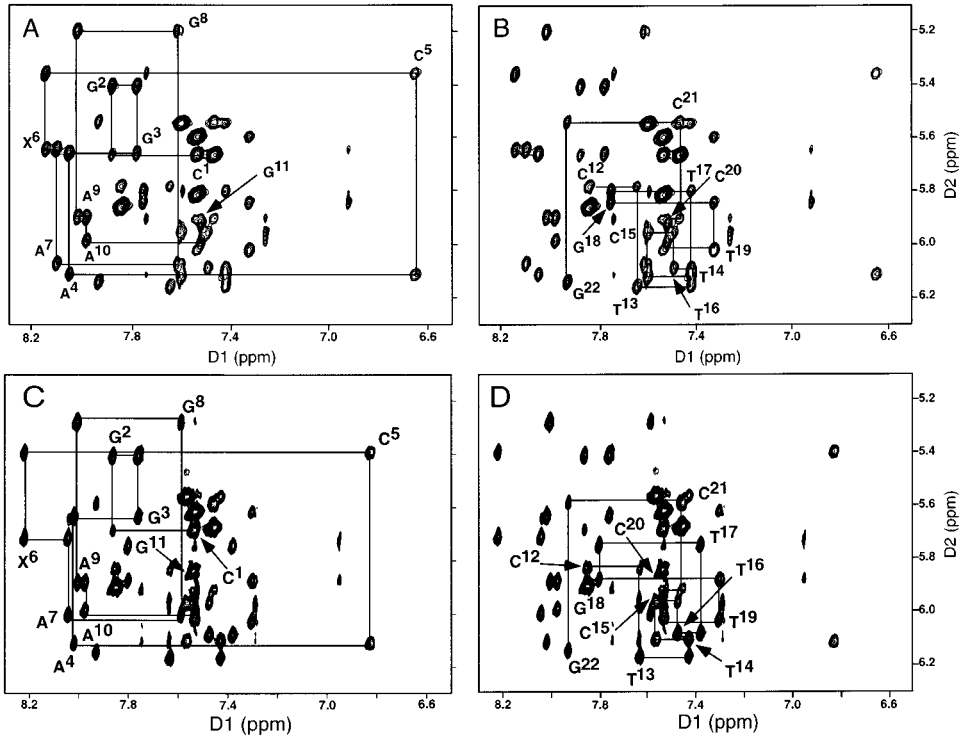


FIGURE 1: Expanded plots of phase-sensitive NOESY spectra in $D_2O$ buffer (pH 7.0) at a mixing time of 250 ms showing sequential NOE connectivities from the aromatic to anomeric protons. (A) Nucleotides $C^1$−$G^{11}$ of the β-R(61,2) adduct. (B) Nucleotides $C^{12}$−$G^{22}$ of the β-R(61,2) adduct. (C) Nucleotides $C^1$−$G^{11}$ of the β-S(61,2) adduct. (D) Nucleotides $C^{12}$−$G^{22}$ of the β-S(61,2) adduct. The base positions are indicated at the intranucleotide cross-peak of the aromatic proton to its own anomeric proton.

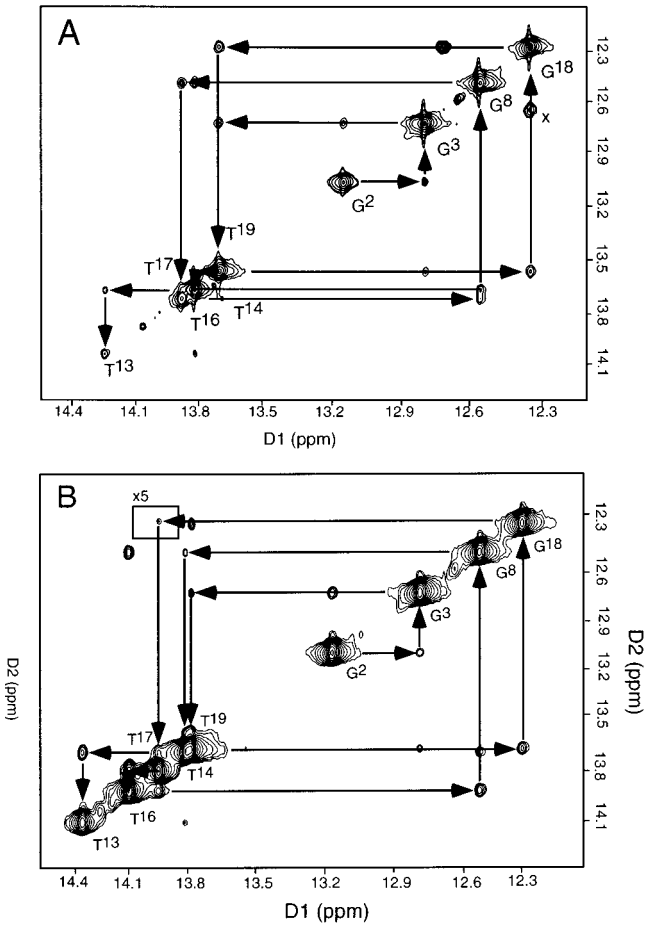


FIGURE 2: Expanded plots of phase-sensitive NOESY spectra (pH 7.0) at a mixing time of 200 ms showing NOE connectivities for the imino protons of base pairs from $G^2$•$C^{21}$ to $A^{10}$•$T^{13}$ for (A) the $\beta$-R(61,2) adduct and (B) the $\beta$-S(61,2) adduct. The peak labeled "x" represents an unidentified cross-peak that may arise from a non-Watson−Crick-bonded structure involving $T^{17}$, as described in the text.

suggested that, irrespective of stereochemistry at the $\beta$-position, the styrene ring was positioned near the $C^5$ aromatic protons.

*Exchangeable Protons*. Spectra of the imino protons from the $\beta$-R(61,2) and $\beta$-S(61,2) diastereomers are shown in Figure 2. For the $\beta$-R(61,2) diastereomer, the $T^{17}$ N3H and $T^{19}$ N3H resonances were superimposed at 13.7 ppm. $T^{17}$ N3H is the imino proton at the modified base pair. This was similar to the unmodified *ras61* oligomer, in which these two imino resonances were separated by only 0.05 ppm (*32*). At the 5′-neighbor base pair $C^5$•$G^{18}$, an unexpected cross-peak was observed between $G^{18}$ N1H and an unidentified resonance at approximately 12.6 ppm (peak x, Figure 2A). The 12.6 ppm resonance exhibited a weak diagonal cross-peak, indicating rapid exchange with solvent. The possibility that this peak arose from a small percentage of a second conformation for $G^{18}$ was discounted because there was no other evidence for a second adduct conformation in the spectra. A more likely possibility is the presence of a small population containing a non-hydrogen-bonded structure involving $T^{17}$, the nucleotide complementary to the modified base $X^6$. This would be consistent with the 12.6 ppm chemical shift and with the rapid exchange of this resonance with solvent. In any event, the observation of the $T^{16}$ N3H−$T^{17}$ N3H cross-peak placed the latter resonance at 13.7 ppm. This suggested that the predominant structure was one in which the $X^6$•$T^{17}$ base pair remained intact, and stacked within the helix.

For the $\beta$-S(61,2) diastereomer, the imino region signals were resolved, although $T^{14}$ N3H and $T^{19}$ N3H were partially overlapped. Nucleotide $G^{18}$ exhibited only the expected cross-peaks, to $T^{17}$ N3H and $T^{19}$ N3H. The unusual feature of the spectrum was the weaker than normal cross-peak between (box x5, Figure 2B) $T^{17}$ N3H and $G^{18}$ N1H. This was the sequential connectivity on the 5′-side of the modified base pair $X^6$•$T^{17}$. This result suggested a greater-than-normal distance between these two protons. Because of the superposition of $T^{17}$ N3H and $T^{19}$ N3H in the spectrum of the $\beta$-R(61,2) diastereomer, it was not possible to determine the magnitude of the anticipated sequential connectivity ($T^{17}$ N3H−$G^{18}$ N1H). This NOE could also be weak or missing in the $\beta$-R(61,2) diastereomer.

*Styrenyl Protons*. For both diastereomers, the styrene aromatic protons were not individually resolved. They were observed as a single resonance at 7.44 ppm integrating to five protons. This result suggests that the styrene ring undergoes rapid flipping on the NMR time scale such that the individual aromatic protons experience a time-averaged chemical shift. Furthermore, the chemical shift environment of the ortho, meta, and para protons of the aromatic ring must be quite similar.

*Chemical Shift Perturbations*. Figure 3 shows the chemical shift differences observed between the unmodified *ras61* oligodeoxynucleotide and the $\beta$-R(61,2) and $\beta$-S(61,2) oligodeoxynucleotides. For both diastereomers, significant upfield chemical shifts were observed for the aromatic protons of nucleotide $C^5$. This is the 5′-neighboring nucleotide to the modified $X^6$. For the $\beta$-R(61,2) adduct, $C^5$ H5 exhibited a 0.7 ppm upfield shift whereas $C^5$ H6 exhibited a 0.4 ppm upfield shift. For the $\beta$-S(61,2) adduct, $C^5$ H5 exhibited a 0.5 ppm upfield shift whereas $C^5$ H6 exhibited a 0.4 ppm upfield shift. These were attributed to ring current shielding effects due to the proximity of the styrene phenyl ring. This was a localized shift. At other sites in both oligodeoxynucleotides, only very small chemical shift effects were noted in the presence of the adduct.

*Styrene−DNA NOEs*. Table 2 shows the NOEs observed between styrene protons and the DNA for both the $\beta$-R(61,2) and $\beta$-S(61,2) diastereomers. In neither did the styrenyl $H_a$ proton exhibit a correlation with DNA protons. For the *S*-diastereomer, the styrenyl $H_{\beta'}$ proton exhibited NOEs with $X^6$ H8, $C^5$ H5, and $C^5$ H6. The $H_{\beta''}$ proton exhibited NOEs with $C^5$ H5 and $C^5$ H6. The unresolved resonances arising from the aromatic protons of the phenyl ring showed a major groove NOE to $T^{16}$ $CH_3$, the nucleotide complementary to the adducted $X^6$. They also exhibited NOEs in the 5′-direction, to $C^5$ H5 and $C^5$ H6. For the $\beta$-R(61,2) diastereomer, the styrenyl $H_{\beta'}$ proton exhibited NOEs with $C^5$ H5 and $C^5$ H6. The $H_{\beta''}$ proton exhibited an NOE to $C^5$ H6. The unresolved resonances arising from the aromatic protons of the phenyl ring exhibited NOEs also in the 5′-direction, to $C^5$ H5, $T^{16}$ $CH_3$, and $C^{15}$ H5.

*Torsion Angle Measurements*. Scalar coupling measurements showed coupling patterns corresponding to the C2′-endo conformation of the sugar rings in all instances. Likewise, measurement of $^1H-^{31}P$ scalar couplings and $^{31}P$ chemical shifts suggested that there was no major perturba-

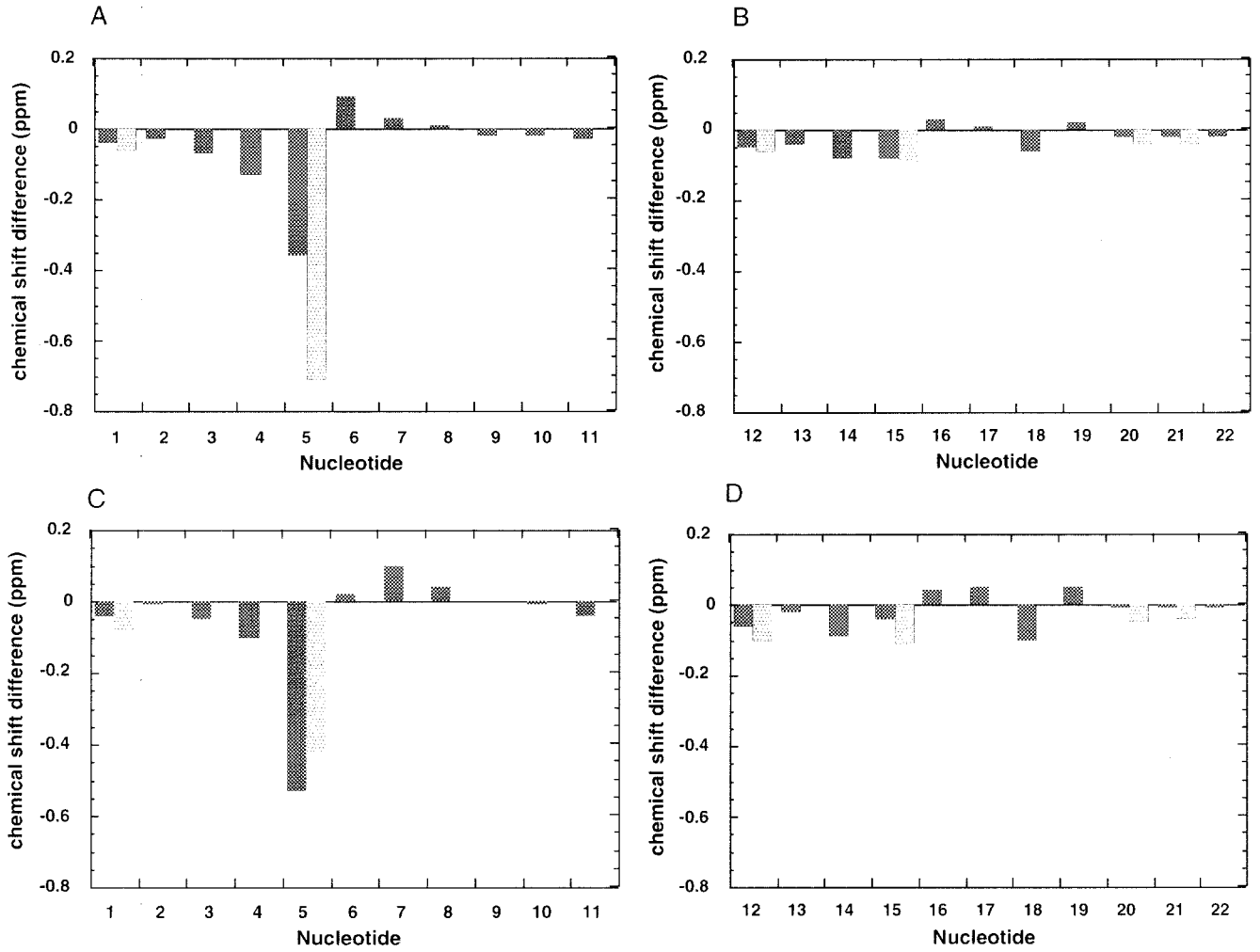


FIGURE 3: Chemical shift differences of aromatic protons of the β-R(61,2) and β-S(61,2) adducts relative to the unmodified ras61 oligodeoxynucleotide. (A) The modified strand of the β-R(61,2) adduct. (B) The complementary strand of the β-R(61,2) adduct. (C) The modified strand of the β-S(61,2) adduct. (D) The complementary strand of the β-S(61,2) adduct. Upfield shifts are negative. For the cytosine residues only, the stippled bars represent the H5 resonance, whereas the cross-hatched bars represent the H6 resonance.

Table 2: Styrene−DNA Cross-Peaks

| | *S*-enantiomer | | | | *R*-enantiomer | | | |
|---|---|---|---|---|---|---|---|---|
| | aromatic | $H_\alpha$ | $H_{\beta'}$ | $H_{\beta''}$ | aromatic | $H_\alpha$ | $H_{\beta'}$ | $H_{\beta''}$ |
| $X^6$ H8 | X | | X | | | | | |
| $C^5$ H5 | X | | X | X | X | | X | |
| $C^5$ H6 | X | | X | X | | | X | X |
| $T^{16}$ Me | X | | | | X | | | |
| $C^{15}$ H5 | | | | | X | | | |

tion in the backbone of the DNA strain. Empirical values were assumed for torsion angles $\epsilon$ and $\gamma$.

*Structural Refinement*. Two starting structures were used, which were built from B-DNA and A-DNA using INSIGHTII (version 97.0) such that the SO moiety was placed into the major groove at $X^6$•$T^{17}$. The calculations were performed using a simulated annealing procedure. Sets of 10 randomly seeded calculations were initiated from both A-form and B-form starting structures. A total of 533 distance restraints were used for the molecular dynamics calculations of the (*S*)-styrenyl-adducted DNA, while 518 distances were used for the (*R*)-styrenyl-adducted oligodeoxynucleotide. The distribution of these restraints is shown in Figure 4. A total of 162 dihedral restraints were obtained for the β-S(61,2)-adducted DNA, while 163 dihedrals were obtained for the β-R(61,2)-adducted DNA.

Figure 5 shows stereoviews of rMD-generated structures based on B-form and A-form DNA. The significant result of the rMD calculations which can be discerned from Figure 5 is the extension of the β-R(61,2) and β-S(61,2) lesions into the major groove of the duplex, with a similar orientation. The β-S(61,2) adduct was refined with somewhat greater precision than the β-R(61,2) adduct. This difference was reflected in the rmsd values listed in Table 3, and was attributed to the superior spectroscopic data which were obtained for the β-S(61,2) adduct. In both cases, the terminal base pairs remained poorly defined, consistent with disorder due to end fraying effects.

For the β-R(61,2) diastereomer, the two starting structures utilized in the rMD calculations differed by an rmsd of 5.9 Å. When compared to the structure that emerged from the rMD calculations, the IniA starting structure differed from ⟨rMDA⟩, with an rmsd of 3.8 Å. When compared to ⟨rMDB⟩, the IniB starting structure yielded an rmsd of 2.0 Å. Thus, the emergent structures were more similar to B-DNA geometry. The rmsd between the averaged refined structures that emerged from the sets of rMD calculations starting from IniA and IniB was 1.4 Å. This suggested that starting from either IniA or IniB, the rMD calculations converged to similar emergent structures. The distribution of the individual

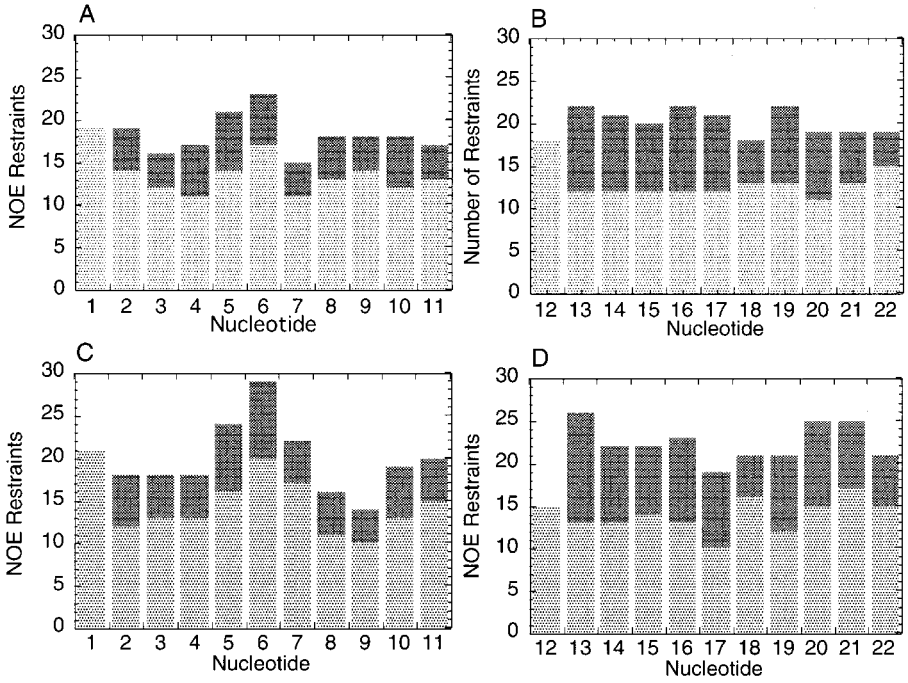


FIGURE 4: Distribution of NOE restraints between nucleotide units of (A) the modified strand of the $\beta$-R(61,2) adduct, (B) the complementary strand of the $\beta$-R(61,2) adduct, (C) the modified strand of the $\beta$-S(61,2) adduct, and (D) the modified strand of the $\beta$-S(61,2) adduct. The dark bars represent internucleotide restraints. The light bars represent intranucleotide restraints.

emergent structures about the average yielded an rmsd value of 1.0 Å. This suggested that the experimental restraints applied to the calculations satisfactorily described a single ensemble of structures.

For the $\beta$-S(61,2) diastereomer, the two starting structures utilized in the rMD calculations differed by an rmsd of 5.9 Å. When compared to the structures that emerged from the rMD calculations, the IniA starting structure differed from ⟨rMDA⟩ with an rmsd of 4.6 Å. When compared to ⟨rMDB⟩, the IniB starting structure yielded an rmsd of 2.5 Å. The emergent structures were therefore more similar to B-DNA geometry. The rmsd between the averaged refined structures that emerged from the sets of rMD calculations starting from IniA and IniB was 1.1 Å. Thus, the emergent structures were relatively independent of the IniA or IniB starting structures. The distribution of the individual emergent structures about the average yielded an rmsd value of $<1.0$ Å, suggesting that the experimental restraints applied to the calculations satisfactorily described a single ensemble of structures.

The accuracy of the emergent structures was assessed by complete relaxation matrix calculations (*49*). These compared theoretical NOE intensities generated from the model structures with experimental data. The results are summarized in Table 4. Figure 6 details the $R_1^x$ values as a function of nucleotide, in the adducted duplexes.

The lower refinement precision observed for the $\beta$-R(61,2) adduct was reflected in its $R_1^x$ values. The overall value of $R_1^x$ for this adduct was $10.3 \times 10^{-2}$. The $R_1^x$ values of starting structures IniA and IniB indicated that the A-DNA starting structure was less consistent with the NMR data than the B-DNA starting structure. Theoretical NOE intensities from each of the refined structures yielded $R_1^x$ values of $8.5 \times 10^{-2}$ for intranucleotide NOEs and $14.6 \times 10^{-2}$ for internucleotide NOEs, which suggest that the refined structures were in better agreement with the data.

Superior $R_1^x$ values were observed for the $\beta$-S(61,2) diastereomer. The $R_1^x$ values of starting structures IniA and IniB also indicated that the A-DNA starting structure was less consistent with the NMR data than the B-DNA starting structure. Theoretical NOE intensities from each of the refined structures yielded $R_1^x$ values of $9.7 \times 10^{-2}$ for intranucleotide NOEs and $11.9 \times 10^{-2}$ for internucleotide NOEs, which suggest that the refined structures were in better agreement with the data. The overall value of $R_1^x$ was $9.3 \times 10^{-2}$. At the nucleotide level, the $R_1^x$ values were found to be between $8 \times 10^{-2}$ and $13 \times 10^{-2}$. This suggested that for the $\beta$-S(61,2) diastereomer, the quality of the refinement was relatively consistent at all positions in the adducted duplex.

## DISCUSSION

Previously, we examined the R(61,2) and R(61,3) adenine $N^6$ adducts of styrene oxide in which the linkage to the DNA was at the α-carbon of the styrenyl moiety (*36*−*38*). The orientation of the R(61,2) and R(61,3) α-(*N*$^6$-adenyl)styrene oxide adducts in duplex DNA was dependent upon the stereochemistry at the α-carbon. The α-R(61,2) adduct was oriented in the 5′-direction in the major groove (*37*), whereas the α-S(61,2) adduct was oriented in the 3′-direction in the major groove (*36*). The $\beta$-R(61,2) and $\beta$-S(61,2) adenine $N^6$ adducts examined in this work differ from the α-R(61,2) and α-S(61,2) adducts in the position of the linkage between the adenine exocyclic amino group and the styrenyl moiety. Moving the linkage from the α- to the $\beta$-carbon of styrene oxide allows for a longer tether between the exocyclic amino group of adenine and the phenyl ring of the styrenyl moiety. This adduct arises solely from rearrangement of an initial $N^1$ adduct by way of a Dimroth rearrangement, in contrast to the $N^6$ α-adduct which arises by a combination of direct $N^6$ and $N^1$ attack followed by rearrangement (*28*, *29*). The results of this work show that the increased tether length

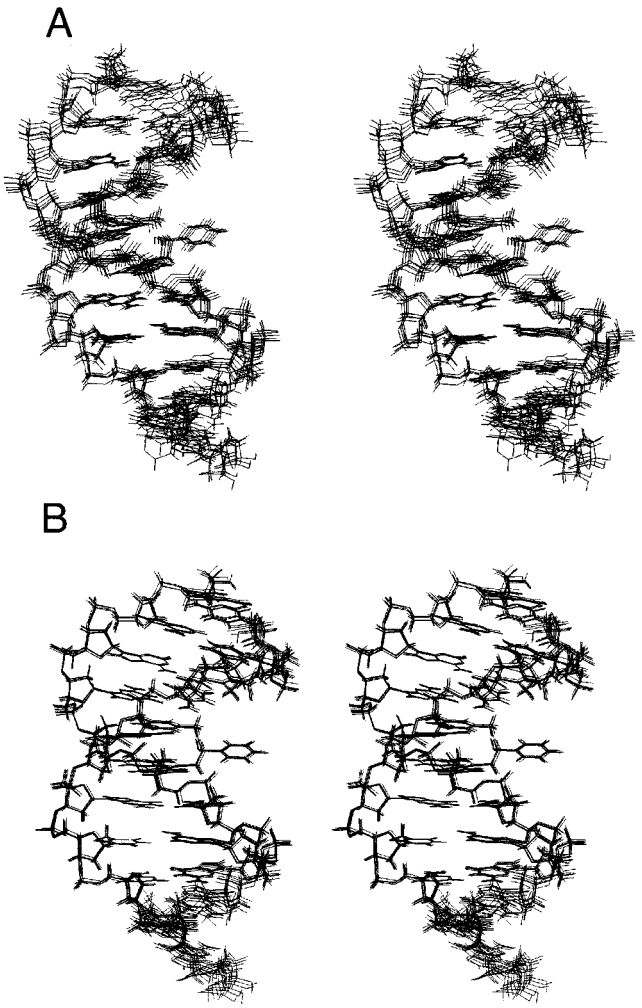


FIGURE 5: Stereoviews of (A) six structures that emerged from randomly seeded rMD calculations for the β-R(61,2) adduct and (B) six structures that emerged from randomly seeded rMD calculations for the β-S(61,2) adduct.

results in two significant changes in the structures of β-adducts as compared to α-adducts. First, it substantially reduces the distortion introduced into the DNA duplex by the β-R(61,2) and β-S(61,2) adducts, as compared to the corresponding α-styrenyl adducts. Second, it mutes the influence of stereochemistry at the α-carbon such that both the β-R(61,2) and β-S(61,2) adducts exhibit similar conformations.

*Minimal Structural Perturbations Induced by the (R)- and (S)-β-Styrenyl Oxide Adducts at Adenine N6*. Perhaps the most significant observation of this work is that in contrast to the α-R(61,2) and α-S(61,2) adducts (*36*−*38*), the β-R(61,2) and β-S(61,2) adducts introduce little or no perturbation into the DNA duplex at the lesion site. The structural refinement of the diasteromeric β-adducts suggests that this is primarily due to the increased tether length between adenine N6 and the phenyl ring of the styrene moiety. This increased tether allows the styrene phenyl ring to be easily accommodated within the major groove, without sterically clashing with the DNA in either the 5′- or 3′-direction. The refined DNA duplex structure remains substantially as in the unmodified ras61 oligodeoxynucleotide (*32*), as shown in Figure 7. This is consistent with NMR spectroscopic data, which show that NOE and *J* couplings

Table 3: Root-Mean-Square (rms) Deviations, Excluding the End Base Pairs, between Various Initial Structures, Intermediate Structures, and Final Average Structures of the *R*- and *S*-Diastereomeric β-Styrenyl Oxide Adducts

| | atomic rms difference (Å) |
|---|---|
| initial structures | |
| $IniA_R$ vs $IniB_R$ | 5.90 |
| $IniA_S$ vs $IniB_S$ | 5.92 |
| rms shifts | |
| $IniA_R$ vs $\langle rMDA_R \rangle$[a] | 3.78 ± 0.49 |
| $IniB_R$ vs $\langle rMDB_R \rangle$[b] | 2.01 ± 0.53 |
| $IniA_S$ vs $\langle rMDA_S \rangle$[a] | 4.58 ± 0.15 |
| $IniB_S$ vs $\langle rMDB_S \rangle$[b] | 2.53 ± 0.17 |
| rms distributions | |
| $\langle rMDA_R \rangle$ vs $\langle rMDA_R \rangle$ | 0.77 ± 0.30 |
| $\langle rMDA_S \rangle$ vs $\langle rMDA_S \rangle$ | 0.64 ± 0.25 |
| $\langle rMDB_R \rangle$ vs $\langle rMDB_R \rangle$ | 1.02 ± 0.35 |
| $\langle rMDB_S \rangle$ vs $\langle rMDB_S \rangle$ | 0.47 ± 0.12 |
| $\langle rMDA_R \rangle$ vs $\langle rMDB_R \rangle$ | 1.37 ± 0.10 |
| $\langle rMDA_S \rangle$ vs $\langle rMDB_S \rangle$ | 1.09 ± 0.17 |
| $\langle rMDA_R \rangle$ vs $rMD_R$[c] | 1.02 ± 0.22 |
| $\langle rMDA_S \rangle$ vs $rMD_S$ | 0.81 ± 0.07 |
| $\langle rMDB_R \rangle$ vs $rMD_R$ | 0.10 ± 0.08 |
| $\langle rMDB_S \rangle$ vs $rMD_S$ | 0.58 ± 0.11 |

[a] ⟨rMDA⟩ represents the set of five structures which emerged from MD calculations starting with IniA. [b] ⟨rMDB⟩ represents the set of five structures which emerged from MD calculations starting from IniB. [c] rMD represents the average minimized structure from all 10 MD calculations. R and S represent the (*R*)-styrene and (*S*)-styrene adducts, respectively.

Table 4: Comparison of Sixth-Root Residual Indices $R_1^x$ for Starting Models and the Resulting rMD Structures[a]

| structure | intraresidue $R_1^x$ | interresidue $R_1^x$ | total $R_1^x$ |
|---|---|---|---|
| $IniA_R$ | 0.152 | 0.297 | 0.193 |
| $IniA_S$ | 0.106 | 0.198 | 0.132 |
| $IniB_R$ | 0.145 | 0.209 | 0.164 |
| $IniB_S$ | 0.108 | 0.131 | 0.115 |
| $rMDA_R$ | 0.084 | 0.136 | 0.099 |
| $rMDA_S$ | 0.097 | 0.119 | 0.104 |
| $rMDB_R$ | 0.080 | 0.134 | 0.095 |
| $rMDB_S$ | 0.098 | 0.117 | 0.104 |
| $rMD_R$ | 0.085 | 0.146 | 0.103 |
| $rMD_S$ | 0.084 | 0.123 | 0.093 |

[a] $R_1^x = \sum|(a_o)_i^{1/6} - (a_c)_i^{1/6}/\sum|(a_o)_i^{1/6}|$, where $a_o$ and $a_c$ are the intensities of observed (non-zero) and calculated NOE cross-peaks, respectively.

in the adducted DNA remain unperturbed. The primary spectroscopic feature of the adducted DNA is a large chemical shift effect observed for the 5′-neighbor cytosine, which is shifted substantially upfield. The refined structures suggest that these upfield chemical shifts can be attributed to ring current shielding from the phenyl ring of the styrene moiety.

The inability to resolve styrenyl ring resonances for either the β-R(61,2) or β-S(61,2) styrenyl oxide adducts was consistent with the conclusion that in both instances, the phenyl ring was undergoing rapid reorientation in the major groove. Consequently, all ring protons existed in indistinguishable chemical shift environments. It was therefore not possible to determine the exact orientation of the phenyl ring in the major groove from NOE data. Potential energy minimization suggested that for both the β-R(61,2) and β-S(61,2) diastereomers, the phenyl ring of the styrene was approximately parallel to the $C^5$ base. This probably accounts for the large chemical shifts observed for $C^5$ H5 and H6

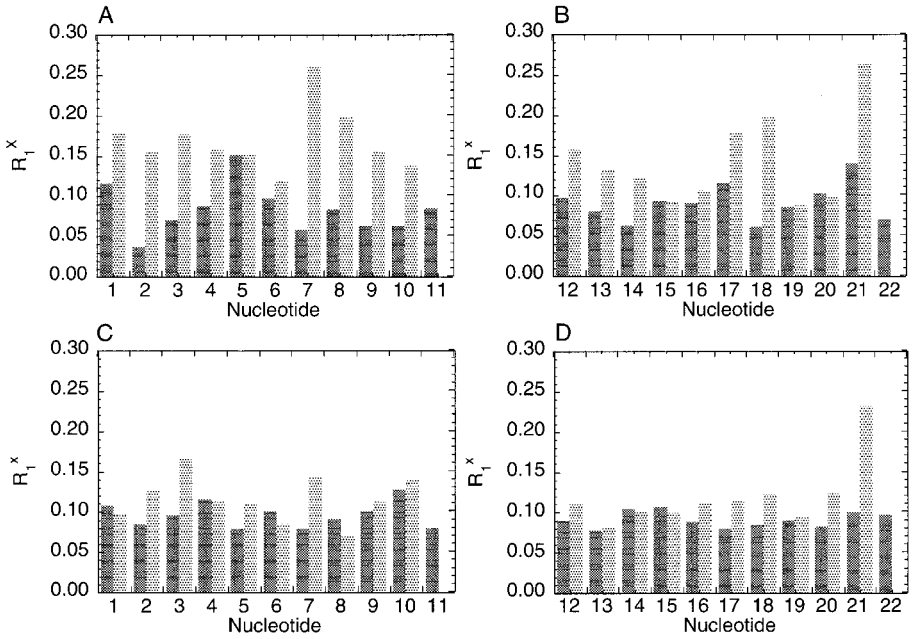


FIGURE 6: Distribution of $R_1^x$ values between nucleotide units of (A) the modified strand of the $\beta$-R(61,2) adduct, (B) the complementary strand of the $\beta$-R(61,2) adduct, (C) the modified strand of the $\beta$-S(61,2) adduct, and (D) the modified strand of the $\beta$-S(61,2) adduct. The dark bars represent intranucleotide $R_1^x$ values. The light bars represent internucleotide $R_1^x$ values.

protons in both. The rapid interconversion of the phenyl rings in the work presented here was in contrast with the slower (NMR time scale) rate of ring flips observed for the α-R(61,2) adduct. In the latter instance, steric hindrance of the styrene ring crowding the 5′-neighbor base pair in the major groove was believed to reduce the rate of ring flips.

*Muted Stereochemical Effects*. One of the characteristic features of adenine $N^6$ styrenyl (*36*−*40*, *57*) and PAH (*58*−*74*) adducts was the role of adduct stereochemistry in determining adduct orientation with respect to the modified adenine base. For the adenine $N^6$ PAH adducts, those having *R*-stereochemistry at the benzylic carbon were found to intercalate 5′ to the lesion site. Those having *S*-stereochemistry at the benzylic carbon were found to be disordered or to prefer intercalation in the 3′-direction. Whether an ordered 3′-intercalated structure was found depended strongly on the arrangement of aromatic rings in the PAH moiety. Benzo[*c*]phenanthrene (*64*) and the bay region benz[*a*]anthracene (*66*) adducts formed ordered 3′-intercalation structures, whereas benzo[*a*]pyrene (*65*) and non-bay region benz[*a*]anthracene (*67*) adducts formed disordered structures. A similar pattern held for the α-styrenyl oxide adducts, which were oriented in the major groove instead of intercalating. For the α-styrenyl adducts, those having *R*-stereochemistry at the α-carbon were oriented in the 5′-direction (*37*), whereas those having *S*-stereochemistry were oriented in the 3′-direction (*36*).

This stereochemical effect is muted in the $\beta$-styrenyl oxide adducts. Structural refinement indicates that irrespective of stereochemistry at the α-carbon atom, the attached styrenyl moiety is positioned in the major groove of the DNA, with little or no steric hindrance. Either diastereomer at the α-carbon is equally well accommodated in the major groove. This contrasts with the corresponding α-R(61,2) and α-S(61,3) adducts. The shorter tether in that case resulted in steric clashing between the phenyl moiety of the styrene and the DNA. This was particularly the case for the α-R(61,2) adduct, in which case the 5′-neighbor was deoxycytosine.

*Biological Implications*. Site-specific mutagenesis studies using an M13 replication vector examined the efficiency of lesion bypass in vivo. The mutation frequencies in *Escherichia coli* arising from replication of the site-specific $\beta$-R(61,2) and $\beta$-S(61,2) adducts as compared to those for the corresponding unadducted DNA were obtained by differential hybridization. The data indicated that no point mutations occurred. The detection limit was $<0.1\%$ frequency. These data suggest that the $\beta$-R(61,2) and $\beta$-S(61,2) adducts are not mutagenic. DNA replication studies in vitro revealed that the $\beta$-R(61,2) and $\beta$-S(61,2) adducts did not block DNA replication. They were readily bypassed by a variety of DNA polymerases (*44*).

The precise manner in which the $\beta$-R(61,2) and $\beta$-S(61,2) adducts interact with the *E. coli* replication complex remains to be determined. Nevertheless, the lack of mutagenicity and facile bypass of these adducts (*44*) seems to be consistent with the present structural studies showing minimal DNA perturbation and unhindered accommodation of the styrene phenyl ring in the major groove. The presence of the relatively small and nondistorting $\beta$-R(61,2) and $\beta$-S(61,2) lesions in the major groove of template DNA evidently does not prevent the correct incorporation of thymidine opposite the modified deoxyadenosine. Guanine N7 lesions introduced by a variety of DNA alkylating agents tend to be nonmutagenic.

The replication fate of these lesions appears to be connected to the tether length between adenine $N^6$ and the styrenyl moiety. In contrast to the $\beta$-R(61,2) and $\beta$-S(61,2) adducts, the α-R(61,2) and α-S(61,2) adducts exhibited biological activity in the M13 replication experiments. For the latter adducts, both adduct structure and mutagenicity were dependent on the chirality of the lesion. In the case of the α-adducts, one mechanism by which the DNA duplex accommodated the steric hindrance of the phenyl ring was by alteration of base stacking and the corresponding base pairing geometry at the lesion site. Site-specific mutagenesis showed that the α-R(61,2) adduct was nonmutagenic and

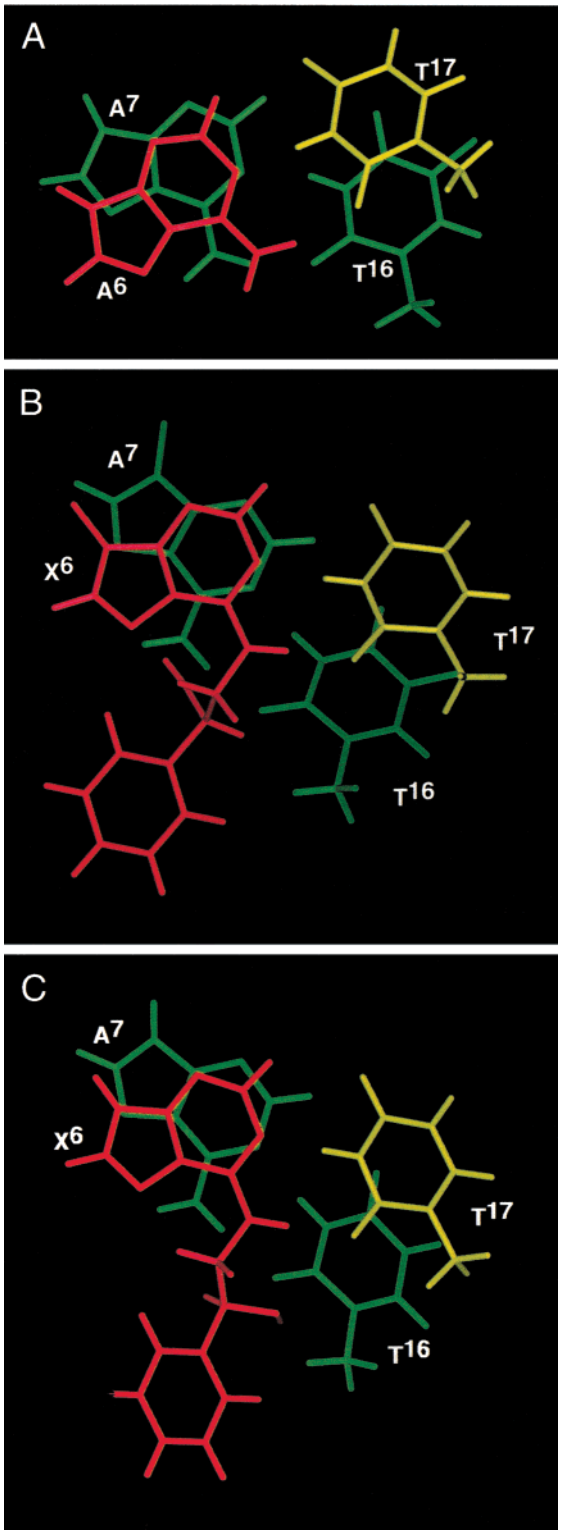


FIGURE 7: Base stacking orientation of the styrenyl moiety at the lesion site as predicted by rMD calculations, as compared to the unmodified ras61 oligodeoxynucleotide duplex. (A) The unmodified ras61 oligodeoxynucleotide. (B) The β-R(61,2) adduct. (C) The β-S(61,2) adduct. In all instances, the $A^7$·$T^{16}$ base pair is green. The adducted nucleotide $X^6$ is red. Nucleotide $T^{17}$ in the complementary strand is yellow. The styrenyl moiety (red) is oriented such that the aromatic ring remains in the major groove and is facing the 5′-direction from the lesion site. The $X^6$·$T^{17}$ base pair is intact.

appeared to be lethal (*33*). Work in vitro showed that polymerization was generally terminated either opposite or one base 3′ to the adduct. Primer extension mediated by HIV-1 reverse transcriptase resulted in stop sites three bases after translesion synthesis but before reaching the end of the template. When replication was restricted to single catalytic cycles, the α-R(61,2) lesion blocked polymerases, limiting the accumulation of fully extended primers. Bypass was facilitated in most cases when excess polymerase was used to drive the reactions. Polymerase β was unable to synthesize full-length products from α-R(61,2)-adducted templates. For the α-R(61,2) adduct, the differing replication results reflected structural differences in the respective primer−template replication complexes, and supported the notion that lesion bypass is polymerase-specific. The slow rate of lesion bypass might enhance the possibility of misincorporation opposite the damage site. The α-S(61,2) adduct was bypassed by all of the above enzymes and was weakly mutagenic. It yielded low levels of A → G mutations (*33*).

The major groove location of the β-R(61,2) and β-S(61,2) adducts reduces biological activity. In contrast, placement of styrene oxide adducts into the minor groove appears to be more deleterious to the cellular replication machinery. Alterations of the structure of potentially critical residues in the HIV-1 reverse transcriptase and its interaction with site-specific and stereospecifically modified DNAs containing the α-*R*- and α-*S*-enantiomers of styrene oxide guanine $N^2$ lesions suggested adduct-induced termination of replication corresponding to the position of the DNA where α-helix H made contact with the minor groove (*75*). Eight mutants of reverse transcriptase in which alternate residues were substituted for $Trp^{266}$ were studied to probe the molecular interactions occurring in critical regions of the minor groove binding track containing $Gly^{262}$ and $Trp^{266}$ (*76*). These enzymes were characterized in primer extension assays in which template DNA was adducted at a single adenine by either α-*R*- or α-*S*-enantiomers of styrene oxide. These lesions failed to block DNA polymerization by wild-type reverse transcriptase, but the $Trp^{266}$ mutants and an alanine mutant of $Gly^{262}$ terminated synthesis on styrene oxide-adducted templates.

*Summary*. The increased tether length of the adenine $N^6$ β-styrene oxide adduct substantially reduces the distortion introduced into the DNA duplex, as compared to that in the adenine $N^6$ α-styrene oxide adducts. Additionally, it mutes the influence of stereochemistry at the α-carbon such that both the β-R(61,2) and β-S(61,2) adducts exhibit similar conformations. The results are correlated with the results of site-specific mutagenesis experiments that revealed the β-R(61,2) and β-S(61,2) adducts were nonmutagenic. Moreover, replication studies in vitro showed that these two adducts did not pose significant replication blocks to a variety of polymerases (*44*).

## ACKNOWLEDGMENT

Dr. Irene S. Zegar, Mr. Jason P. Weisenseel, and Mr. Markus Voehler assisted with NMR spectroscopy and structural refinement. Dr. Gary J. Latham and Professor R. Stephen Lloyd (The University of Texas Medical Branch, Galveston, TX) provided helpful discussions. We especially thank Dr. Nathalie Schnetz-Boutaud and Ms. Tandace Scholdberg for assistance with preparation of the manuscript.

## SUPPORTING INFORMATION AVAILABLE

$^1$H NMR chemical shift assignments (Tables S1 and S2), the experimental distances and classes of restraints for the $\beta$-R(61,2) and $\beta$-S(61,2) oligodeoxynucleotides (Table S3), and force field parametrization values used for styrene oxide (Figure S1). This material is available free of charge via the Internet at http://pubs.acs.org.

## REFERENCES


1. de Meester, C., Poncelet, F., Roberfroid, M., Rondelet, J., and Mercier, M. (1977) *Mutat. Res. 56*, 147−152.
2. Wade, D. R., Airy, S. C., and Sinsheimer, J. E. (1978) *Mutat. Res. 58*, 217−223.
3. Sugiura, K., and Goto, M. (1981) *Chem.-Biol. Interact. 35*, 71−91.
4. Bonatti, S., Abbondandolo, A., Corti, G., Fiorio, R., and Mazzaccaro, A. (1978) *Mutat. Res. 52*, 295−300.
5. Ott, M. G., Kolesar, R. C., Schamweber, H. C., Schneider, E. J., and Venable, J. R. (1980) *J. Occup. Med. 22*, 445−460.
6. Hodgson, J. T., and Jones, P. D. (1985) *J. Work Environ. 11*, 347−352.
7. Matanoski, G. M., and Schwarts, L. (1987) *J. Occup. Med. 29*, 675−680.
8. Wong, O. (1990) *J. Ind. Med. 47*, 753−762.
9. McConnell, E. E., and Swenberg, J. A. (1994) *Crit. Rev. Toxicol. 24* (Suppl.), S49−S55.
10. Harris, C., Philpot, R. M., Hernandez, O., and Bend, J. R. (1986) *J. Pharmacol. Exp. Ther. 236*, 144−149.
11. Foureman, G. L., Harris, C., Guengerich, F. P., and Bend, J. R. (1989) *J. Pharmacol. Exp. Ther. 248*, 492−497.
12. Elovaara, E., Engstrom, K., Nakajima, T., Park, S. S., Gelboin, H. V., and Vainio, H. (1991) *Xenobiotica 21*, 651−661.
13. Himmelstein, M. W., Acquavella, J. F., Recio, L., Medinsky, M. A., and Bond, J. A. (1997) *Crit. Rev. Toxicol. 27*, 1−108.
14. Guengerich, F. P. (1992) *FASEB J. 6*, 745−748.
15. Nelson, D. R., Kamataki, T., Waxman, D. J., Guengerich, F. P., Estabrook, R. W., Feyereisen, R., Gonzalez, F. J., Coon, M. J., Gunsalus, I. C., Goto, O., Okuda, K., and Nebert, D. W. (1993) *DNA Cell Biol. 10*, 1−51.
16. Nakajima, T., Elovaara, E., Gonzalez, F. J., Gelboin, H. V., Raunio, H., Pelkonen, O., Vainio, H., and Aoyama, T. (1994) *Chem. Res. Toxicol. 7*, 891−896.
17. Nakajima, T., Wang, R.-S., Elovaara, E., Gonzalez, F. J., Gelboin, H. V., Vainio, H., and Aoyama, T. (1994) *Biochem. Pharmacol. 48*, 637−642.
18. Norppa, H., Sorsa, M., Pfaffli, P., and Vainio, H. (1980) *Carcinogenesis 1*, 357−361.
19. Norppa, H., Hemminki, K., Sorsa, M., and Vainio, H. (1981) *Mutat. Res. 91*, 243−250.
20. Horvath, E., Prongracz, K., Rappaport, S., and Bodell, W. J. (1994) *Carcinogenesis 15*, 1309−1315.
21. Vodicka, P., Vodickova, L., and Hemminki, K. (1993) *Carcinogenesis 14*, 2059−2061.
22. Vodicka, P., Vodickova, L., Trejbalova, K., Scram, R. J., and Hemminki, K. (1994) *Carcinogenesis 15*, 1949−1953.
23. Vodicka, P., Bastlova, T., Vodickova, L., Peterkova, K., Lambert, B., and Hemminki, K. (1995) *Carcinogenesis 16*, 1473−1481.
24. Bastlova, T., Vodicka, P., Peterkova, K., Hemminki, K., and Lambert, B. (1995) *Carcinogenesis 16*, 2357−2362.
25. Bastlova, T., and Podlutsky, A. (1996) *Mutagenesis 11*, 581−591.
26. Savela, K., and Hemminki, K. (1986) *Arch. Toxicol. 9* (Suppl.), 281−285.
27. Barlow, T., Takeshita, J., and Dipple, A. (1998) *Chem. Res. Toxicol. 11*, 838−845.
28. Qian, C., and Dipple, A. (1995) *Chem. Res. Toxicol. 8*, 389−395.
29. Kim, H. Y., Finneman, J. I., Harris, C. M., and Harris, T. M. (2000) *Chem. Res. Toxicol. 13*, 625−637.
30. Longnecker, D. S., and Terhune, P. G. (1998) *Pancreas 17*, 323−324.
31. Barbacid, M. (1987) *Annu. Rev. Biochem. 56*, 779−827.
32. Feng, B., and Stone, M. P. (1995) *Chem. Res. Toxicol. 8*, 821−832.
33. Latham, G. J., Zhou, L., Harris, C. M., Harris, T. M., and Lloyd, R. S. (1993) *J. Biol. Chem. 268*, 23427−23434.
34. Latham, G. J., and Lloyd, R. S. (1994) *J. Biol. Chem. 269*, 28527−28530.
35. Latham, G. J., Harris, C. M., Harris, T. M., and Lloyd, R. S. (1995) *Chem. Res. Toxicol. 8*, 422−430.
36. Feng, B., Voehler, M. W., Zhou, L., Passarelli, M., Harris, C. M., Harris, T. M., and Stone, M. P. (1996) *Biochemistry 35*, 7316−7329.
37. Feng, B., Zhou, L., Passarelli, M., Harris, C. M., Harris, T. M., and Stone, M. P. (1995) *Biochemistry 34*, 14021−14036.
38. Stone, M. P., and Feng, B. (1996) *Magn. Reson. Chem. 34*, S105−S114.
39. Painter, S. L., Zegar, I. S., Tamura, P. J., Bluhm, S., Harris, C. M., Harris, T. M., and Stone, M. P. (1999) *Biochemistry 38*, 8635−8646.
40. Simeonov, M. F., Tamura, P. J., Wilkinson, A. S., Harris, C. M., Harris, T. M., and Stone, M. P. (2000) *Biochemistry 39*, 924−937.
41. Harris, C. M., Zhou, L., Strand, E. A., and Harris, T. M. (1991) *J. Am. Chem. Soc. 113*, 4328−4329.
42. Chary, P., Latham, G. J., Robberson, D. L., Kim, S. J., Han, S., Harris, C. M., Harris, T. M., and Lloyd, R. S. (1995) *J. Biol. Chem. 270*, 4990−5000.
43. McNees, A. G., O'Donnell, M., Horton, P. H., Kim, H. Y., Kim, S. J., Harris, C. M., Harris, T. M., and Lloyd, R. S. (1997) *J. Biol. Chem. 272*, 33211−33219.
44. Kanuri, M., Harris, C. M., Harris, T. M., and Lloyd, R. S. (2001) *Environ. Mol. Mutagen. 38* (in press).
45. Borer, P. N. (1975) in *Handbook of Biochemistry and Molecular Biology*, CRC Press, Cleveland.
46. Piotto, M., Saudek, V., and Sklenar, V. (1992) *J. Mol. Biol. 6*, 661−665.
47. Arnott, S., and Hukins, D. W. L. (1972) *Biochem. Biophys. Res. Commun. 47*, 1504−1509.
48. Borgias, B. A., and James, T. L. (1990) *J. Magn. Reson. 87*, 475−487.
49. Liu, H., Tonelli, M., and James, T. L. (1996) *J. Magn. Reson., Ser. B 111*, 85−89.
50. Gorenstein, D. G., Schroeder, S. A., Fu, J. M., Metz, J. T., Roongta, V., and Jones, C R. (1988) *Biochemistry 27*, 7223−7237.
51. Brunger, A. T. (1992) in *X-Plor. Version 3.1. A System for X-ray Crystallography and NMR*, Yale University Press, New Haven, CT.
52. Brooks, B. R., Bruccoleri, R. E., Olafson, B. D., States, D. J., Swaminathan, S., and Karplus, M. (1983) *J. Comput. Chem. 4*, 187−217.
53. Clore, G. M., Gronenborn, A. M., Carlson, G., and Meyer, E. F. (1986) *J. Mol. Biol. 190*, 259−267.
54. Keepers, J. W., and James, T. L. (1984) *J. Magn. Reson. 57*, 404−426.
55. Reid, B. R. (1987) *Q. Rev. Biophys. 20*, 2−28.
56. Patel, D. J., Shapiro, L., and Hare, D. (1987) *Q. Rev. Biophys. 20*, 35−112.
57. Setayesh, F. R., DeCorte, B. L., Horton, P., Harris, C. M., Harris, T. M., and Stone, M. P. (1998) *Chem. Res. Toxicol. 11*, 766−777.
58. Zegar, I. S., and Stone, M. P. (1996) *Chem. Res. Toxicol. 9*, 114−125.
59. Tan, J., Geacintov, N. E., and Broyde, S. (2000) *Chem. Res. Toxicol. 13*, 811−822.
60. Schwartz, J. L., Rice, J. S., Luxon, B. A., Sayer, J. M., Xie, G., Yeh, H. J., Liu, X., Jerina, D. M., and Gorenstein, D. G. (1997) *Biochemistry 36*, 11069−11076.
61. Volk, D. E., Rice, J. S., Luxon, B. A., Yeh, H. J., Liang, C., Xie, G., Sayer, J. M., Jerina, D. M., and Gorenstein, D. G. (2000) *Biochemistry 39*, 14040−14053.
62. Zegar, I. S., Chary, P., Jabil, R. J., Tamura, P. J., Johansen, T. N., Lloyd, R. S., Harris, C. M., Harris, T. M., and Stone, M. P. (1998) *Biochemistry 37*, 16516−16528.

63. Cosman, M., Fiala, R., Hingerty, B. E., Laryea, A., Lee, H., Harvey, R. G., Amin, S., Geacintov, N. E., Broyde, S., and Patel, D. (1993) *Biochemistry 32*, 2488−2497.
64. Cosman, M., Laryea, A., Fiala, R., Hingerty, B. E., Amin, S., Geacintov, N. E., Broyde, S., and Patel, D. J. (1995) *Biochemistry 34*, 1295−1307.
65. Geacintov, N. E., Cosman, M., Hingerty, B. E., Amin, S., Broyde, S., and Patel, D. J. (1997) *Chem. Res. Toxicol. 10*, 111−146.
66. Li, Z., Kim, H. Y., Tamura, P. J., Harris, C. M., Harris, T. M., and Stone, M. P. (1999) *Biochemistry 38*, 16045−16057.
67. Li, Z., Kim, H. Y., Tamura, P. J., Harris, C. M., Harris, T. M., and Stone, M. P. (1999) *Biochemistry 38*, 14820−14832.
68. Li, Z., Mao, H., Kim, H. Y., Tamura, P. J., Harris, C. M., Harris, T. M., and Stone, M. P. (1999) *Biochemistry 38*, 2969−2981.
69. Schurter, E. J., Sayer, J. M., Oh-hara, T., Yeh, H. J. C., Yagi, H., Luxon, B. A., Jerina, D. M., and Gorenstein, D. G. (1995) *Biochemistry 34*, 9009−9020.
70. Schurter, E. J., Yeh, H. J. C., Sayer, J. M., Lakshman, M. K., Yagi, H., Jerina, D. M., and Gorenstein, D. G. (1995) *Biochemistry 34*, 1364−1375.
71. Yeh, H. J. C., Sayer, J. M., Liu, X., Altieri, A. S., Byrd, R. A., Lakshman, M. K., Yagi, H., Schurter, E. J., Gorenstein, D. G., and Jerina, D. M. (1995) *Biochemistry 34*, 13570−13581.
72. Suri, A. K., Mao, B., Amin, S., Geacintov, N. E., and Patel, D. J. (1999) *J. Mol. Biol. 292*, 289−307.
73. Pradhan, P., Tirumala, S., Liu, X., Sayer, J. M., Jerina, D. M., and Yeh, H. J. (2001) *Biochemistry 40*, 5870−5881.
74. Li, Z., Tamura, P. J., Wilkinson, A. S., Harris, C. M., Harris, T. M., and Stone, M. P. (2001) *Biochemistry 40*, 6743−6755.
75. Forgacs, E., Latham, G., Beard, W. A., Prasad, R., Bebenek, K., Kunkel, T. A., Wilson, S. H., and Lloyd, R. S. (1997) *J. Biol. Chem. 272*, 8525−8530.
76. Latham, G. J., Forgacs, E., Beard, W. A., Prasad, R., Bebenek, K., Kunkel, T. A., Wilson, S. H., and Lloyd, R. S. (2000) *J. Biol. Chem. 275*, 15025−15033.

BI010564V